5580 *Chem. Mater.* **2010,** *22,* 5580–5587
DOI:10.1021/cm1019348

CHEMISTRY OF MATERIALS
Article

Noncentrosymmetric Cation Order in the Cubic Perovskite $Ba_4CaFe_3O_{9.5}$

Sarah A. Turp,[†] Joanna Hargreaves,[†] Jaewook Baek,[‡] P. Shiv Halasyamani,[‡] and Michael A. Hayward*,[†]

[†]*Department of Chemistry, University of Oxford, Inorganic Chemistry Laboratory, South Parks Road, Oxford, OX1 3QR, United Kingdom., and* [‡]*Department of Chemistry, University of Houston, 136 Fleming Building, Houston, Texas 77204-5003*

Received July 12, 2010. Revised Manuscript Received August 25, 2010

The syntheses and characterization of the acentric, B-cation ordered phase $Ba_4CaFe_3O_{9.5}$ and a topotactically oxidized product $Ba_4CaFe_3O_{10.7}$ are reported. Utilizing electron diffraction and neutron powder diffraction data, cation ordered structures based on a cubic perovskite lattice were refined for $Ba_4CaFe_3O_{9.5}$ (space group $I2_12_12_1$, $a = 8.234(1)$ Å, $b = 8.213(1)$ Å, $c = 34.622(7)$ Å) and $Ba_4CaFe_3O_{10.7}$ (space group $I\bar{4}2d$ $a = 8.1821(4)$ Å, $c = 32.3105(19)$ Å) The two $Ba_4CaFe_3O_{12-x}$ phases exhibit complex structures in which Ca^{2+} and Fe^{3+} are ordered over the B-sites of the cubic perovskite lattice. This order results in the loss of structural inversion symmetry, thus the resulting cation ordered $Ba_4CaFe_3O_{12-x}$ phases are both magnetic and acentric making them good candidates for multiferroic behavior. Further structural analysis reveals the complex cation order is induced through a combination of factors: the different coordination preferences of Ca^{2+} and Fe^{3+}, anion vacancy ordering, and the need to minimize lattice strain. The general applicability of this synthetic strategy for the preparation of cation ordered materials is discussed.

Introduction

Complex transition metal oxide phases based on the ABO_3 cubic perovskite structure have received considerable attention attributable to the wide range of correlated electronic properties they exhibit.[1] These properties are accompanied by a flexible and diverse chemistry that allows a wide variety of different metal cations to be accommodated within the simple structural lattice, offering chemists numerous opportunities to manipulate and tune the chemical, structural and physical behavior of perovskite phases via cation substitutions. Partial substitution of one cation for another not only allows the valence electron count of phases to be adjusted, it also introduces the possibility of ordering cations within an expanded perovskite lattice as exhibited in its most simple form by $AA'B_2O_6$ and $A_2BB'O_6$ "double perovskite" phases (Figure 1a,b). This ordering of cations provides another vector by which the properties of materials can be tuned as A- and B-cation ordered phases often exhibit significantly different physical behavior to the equivalent cation disordered phases. This effect is demonstrated by magnetoresistive behavior of cation ordered Sr_2FeMoO_6,[2] and the different ferromagnetic ordering temperatures exhibited by A-cation ordered $LaBaMn_2O_6$ and the A-cation disordered analogue $La_{0.5}Ba_{0.5}MnO_3$.[3]

In the search for materials exhibiting complex electronic behavior, chemists have studied phases with more elaborate cation ordering schemes, such as the 3:1 B-site cation order exhibited by $Ba_4LiSb_3O_{12}$ and $(La_{0.5}Sr_{0.5})_4Ti_3CuO_{12}$ (Figure 1c,d).[4,5] However the preparation of phases with complex cation order is challenging, and it is fair to say that perovskite phases with even simple cation ordering schemes are rare. This is because under the synthesis conditions typically employed to prepare complex oxides, entropy makes a dominant contribution to the thermodynamic competition between possible structure types and cation arrangements, so statistically disordered cation arrangements are strongly favored. To overcome this entropically driven preference for disorder, a strong enthalpic motivation to form ordered phases must be provided. In the case of oxygen stoichiometric double perovskites, this enthalpic motivation can be provided by a large difference in charge and/or size between the cations to be ordered. Ordered structures are favored in this situation, i.e., dissimilar cation charge and/or size, because they have better local charge neutrality and lower lattice strain than disordered structures.[6,7] However, the requirement that the cations to be ordered are very dissimilar significantly restricts the chemical diversity of cation ordered phases which can be prepared.

*Corresponding author. Tel: +44 1865 272623. Fax: +44 1865 272690. E-mail: michael.hayward@chem.ox.ac.uk.

(1) Cooper, S. L.; Egami, T.; Goodenough, J. B.; Zhou, J.-S. *Localized to Itinerant Electronic Transition in Perovskite Oxides*; Springer-Velang: Berlin, 2001.
(2) Meneghini, C.; Sugata, Ray; Liscio, F.; Bardelli, F.; Mobilio, S.; Sarma, D. D. *Phys. Rev. Lett.* **2009**, *103*, 46403.
(3) Millange, F.; Caignaert, V.; Domenges, B.; Raveau, B.; Suard, E. *Chem. Mater.* **1998**, *10*, 1974.
(4) Jacobson, A. J.; Collins, B. M.; Fender, B. E. F. *Acta Crystallogr., Sect. B: Strucut. Sci.* **1974**, *30*, 1705.
(5) Sivakumar, T.; Ramesha, K.; Lofland, S. E.; Ramanujachary, K. V.; Subbanna, G. N.; Gopalakrishnan, J. *Inorg. Chem.* **2004**, *43*, 1875.
(6) Anderson, M. T.; Greenwood, K. B.; Taylor, G. A.; Poeppelmeier, K. R. *Prog. Solid St. Chem.* **1993**, *22*, 197.
(7) King, G.; Woodward, P. M. *J. Mater. Chem.* **2010**, *20*, 5785.

Published on Web 09/07/2010

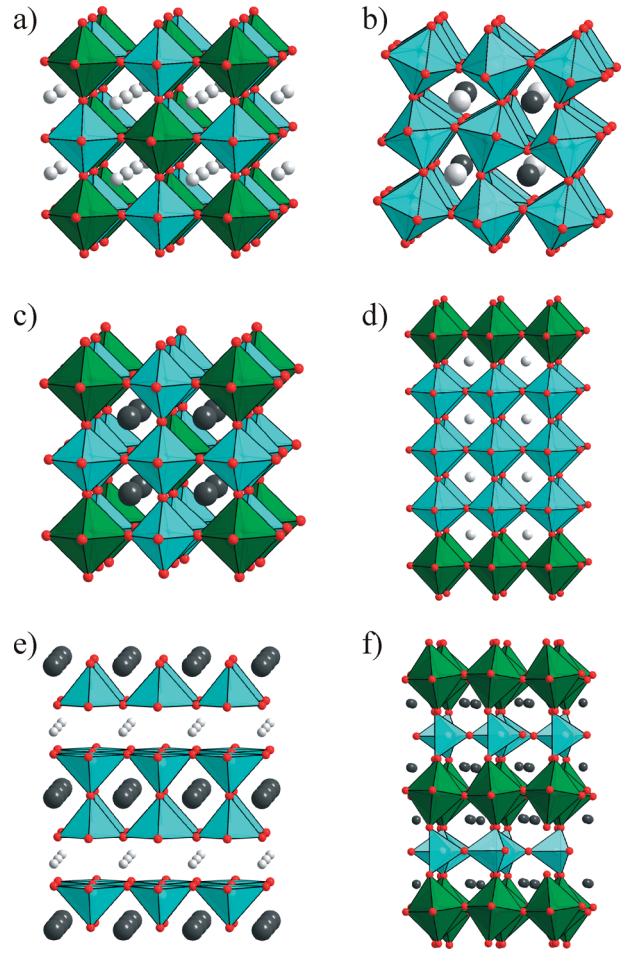

Figure 1. (a) The "rock salt" B-cation order of $A_2BB'O_6$; (b) the A-cation order in $AA'B_2O_6$ $CaFeTi_2O_6$. The 3:1 B-cation order in (c) $Ba_4LiSb_3O_{12}$ and (d) $(La_{0.5}Sr_{0.5})_4Ti_3CuO_{12}$. The combined anion vacancy and cation order in (e)$YBaCo_2O_5$ and (f) Ca_2MnAlO_5.

An alternative strategy that can be employed to encourage cation order uses the observation that some cations favor particular coordination numbers and geometries, attributable to size or crystal field considerations. The cubic perovskite structure can accommodate large numbers of anion vacancies without incurring significant energetic penalties.[8,9] By ordering these anion vacancies within the structure, A- and B-cation sites of different coordination number and geometry can be created encouraging the segregation and ordering of cations. Such a mechanism can be seen at work in the A-cation ordered, anion deficient structures of $LnBaM_2O_{6-x}$ (Ln = Y, lanthanide; M = Mn, Fe, Co [10−12]) phases in which anion vacancy order and cation order combine to produce a structure in which the large Ba^{2+} cation is accommodated within a 12-coordinate site, with the smaller Ln^{3+} ion in an 8-coordinate site (Figure 1e). Analogous B-cation order can also be induced by the introduction of anion vacancies, as demonstrated by cation ordered $A_2BB'O_5$ phases that adopt the brownmillerite type structures.[8] In the example shown in Figure 1f, it can be seen that the Al^{3+}/Mn^{3+} B-site cation order in Ca_2MnAlO_5 is driven by the favorability of locating the relatively small Al^{3+} cation on the small tetrahedral site rather than the large octahedral site within the structure. Likewise, the larger, Jahn−Teller distorted Mn^{3+} cation gains additional lattice and crystal field energy by being located on the distorted octahedral site within the structure.[13]

Here we describe $Ba_4CaFe_3O_{9.5}$ a 3:1 B-site ordered cubic perovskite in which complex cation order is induced by a high concentration of anion vacancies. In this instance the phase adopts a novel cation ordering pattern which breaks the inversion symmetry of the simple cubic perovskite structure allowing the material to exhibit "noncentric" properties, such as second harmonic generation, that are forbidden to centrosymmetric materials.

Experimental Section

Synthesis. Samples of $Ba_4CaFe_3O_{9.5}$ were prepared via standard ceramic synthesis. Suitable stoichiometric ratios of $BaCO_3$ (99.997%), Fe_2O_3 (99.998%), and $CaCO_3$ (99.999%) were ground together and heated at 1000 °C in air to decompose the carbonates. The samples were then pressed into 13 mm pellets and heated under argon for two periods of 40 h at a temperature of 1250 °C. A sample of $Ba_4CaFe_3O_{9.5+x}$ was prepared by heating a preprepared sample of $Ba_4CaFe_3O_{9.5}$ under flowing oxygen at 400 °C for 10 h.

Characterization. X-ray powder diffraction data were collected using a PANalytical X'Pert diffractometer incorporating an X'celerator position sensitive detector (monochromatic Cu $K_{\alpha 1}$ radiation). Neutron powder diffraction data were collected using the POLARIS diffractometer at the ISIS neutron source, UK. Data were collected from samples contained in vanadium cans sealed under argon with a copper gasket. Rietveld profile refinements were performed using the GSAS suite of programs.[14] Electron diffraction patterns were collected from samples supported on lacy carbon grids (deposited from suspension in methanol) using a JEOL 2000FX microscope operating at 200KV. Average iron oxidation states in all phases were determined by iodometric titration. Samples were dissolved in HCl containing an excess of KI and the liberated I_2 was titrated with $Na_2S_2O_3$.

Magnetization data were collected in the temperature range $300 < T\ (K) < 800$ in an applied magnetic field of 1000 Oe, from samples sealed in within Pyrex tubes, utilizing a high-temperature insert to the magnetometer.

Second Harmonic Generation. Powder SHG measurements were performed on a modified Kurtz-NLO system[15] using a pulsed Nd:YAG laser with a wavelength of 1064 nm. A detailed description of the equipment and methodology has been published elsewhere.[16] As the powder SHG efficiency has been

(8) Antipov, E. V.; Abakumov, A. M.; Istomin, S. Y. *Inorg. Chem.* **2008**, *47*, 8543.
(9) Anderson, M. T.; Vaughey, J. T.; Poeppelmeier, K. R. *Chem. Mater.* **1993**, *5*, 151.
(10) Millange, F.; Suard, E.; Caignaert, V.; Raveau, B. *Mater. Res. Bull.* **1999**, *34*, 1.
(11) Woodward, P. M.; Karen, P. *Inorg. Chem.* **2003**, *42*, 1121.
(12) Vogt, T.; Woodward, P. M.; Karen, P.; Hunter, B. A.; Henning, P.; Moodenbaugh, A. R. *Phys. Rev. Lett.* **2000**, *84*, 2969.
(13) Wright, A. J.; Palmer, H. M.; Anderson, P. A.; Greaves, C. *J. Mater. Chem.* **2002**, *12*, 978.
(14) Larson, A. C.; Von Dreele, R. B. *General Structural Analysis System*; Los Alamos National Laboratory Report LAUR 86−748; Los Alamos National Laboratory: Los Alamos, NM, 2000.
(15) Kurtz, S. K.; Perry, T. T. *J. Appl. Phys.* **1968**, *39*, 3798.
(16) Ok, K. M.; Chi, E. O.; Halasyamani, P. S. *Chem. Soc. Rev.* **2006**, *35*, 710.

shown to depend strongly on particle size,[15] the reported materials were ground and sieved into distinct particle size ranges (<20, 20−45, 45−63, 63−75, 75−90, >90 μm). Relevant comparisons with known SHG materials were made by grinding and sieving crystalline α-SiO_2 and $LiNbO_3$ into the same particle size ranges. No index matching fluid was used in any of the experiments.

Results

Characterization of $Ba_4CaFe_3O_{12-x}$ Phases. Iodometric titrations of the "as-made" and oxidized $Ba_4CaFe_3O_{12-x}$ phases indicated average iron oxidation states of +3.02(2) and 3.81(2) respectively consistent with an overall stoichiometries of $Ba_4CaFe_3O_{9.53(3)}$ and $Ba_4CaFe_3O_{10.71(3)}$ respectively. X-ray powder diffraction data collected from $Ba_4CaFe_3O_{9.5}$ could be indexed with a primitive orthorhombic cell ($a \approx 4.08$ Å $b \approx 4.07$ Å $c \approx 4.30$ Å), whereas data collected from $Ba_4CaFe_3O_{10.7}$ were consistent with a tetragonal cell ($a \approx 4.09$ Å $c \approx 4.03$ Å).

The intensity distributions of the X-ray diffraction data collected from both $Ba_4CaFe_3O_{12-x}$ phases are consistent with cubic perovskite type structures of the form $BaCa_{0.25}Fe_{0.75}O_{3-x}$. However, electron diffraction (Figure 2) and neutron diffraction data collected from both $Ba_4CaFe_3O_{9.5}$ and $Ba_4CaFe_3O_{10.7}$ show a series of additional diffraction reflections indicating a $2 \times 2 \times 8$ geometric expansion of the simple perovskite unit cell. The unit-cell expansion is indicative of calcium−iron cation ordering on the B-sites of the cubic perovskite structure. The similarity of the unit cells of the two $Ba_4CaFe_3O_{12-x}$ phases, and the fact that $Ba_4CaFe_3O_{10.7}$ is prepared by the low temperature oxidation of $Ba_4CaFe_3O_{9.5}$, suggests that $Ba_4CaFe_3O_{10.7}$ is a topotactically oxidized form of $Ba_4CaFe_3O_{9.5}$. That is to say that the arrangement of cations in $Ba_4CaFe_3O_{9.5}$ is conserved in the structure of $Ba_4CaFe_3O_{10.7}$; the oxidation simply fills some of the anion vacancies in the $Ba_4CaFe_3O_{12-x}$ phase. This means the two $Ba_4CaFe_3O_{12-x}$ phases have the same ordered arrangement of metal cations within their respective crystal structures. By initially focusing on the structure determination of the high-symmetry oxidized phase ($Ba_4CaFe_3O_{10.7}$), the structure of this cation ordered lattice can be more easily determined and used as a starting point of the refinement of the more complex, lower-symmetry structure of $Ba_4CaFe_3O_{9.5}$.

Structural Characterization of $Ba_4CaFe_3O_{10.7}$. The reflection conditions derived from the electron (Figure 2a,b) and neutron diffraction data collected at 298 K from $Ba_4CaFe_3O_{10.7}$ are hkl, $h+k+l = 2n$; hhl, $2h+l = 4n$; $hh0$, $h = 2n$; $h00$, $h = 2n$; $0k0$, $k = 2n$; $00l$, $l = 4n$. These reflection conditions correspond to the extinction symbol $I\_\_d$, corresponding to the possible space groups $I4_1md$ and $I\bar{4}2d$. The observed $2 \times 2 \times 8$ unit-cell expansion relative to the simple cubic perovskite structure suggests the structure of $Ba_4CaFe_3O_{10.7}$ consists of a Ba_4O_{4-x}−$CaFe_3O_{8-x}$−Ba_4O_{4-x}−$CaFe_3O_{8-x}$ stacking sequence up the c-axis in an analogy to the AO−BO_2−AO−BO_2 stacking sequence of the ABO_3 perovskites. The 2×2 cell expansion in the ab plane is consistent with cation ordered

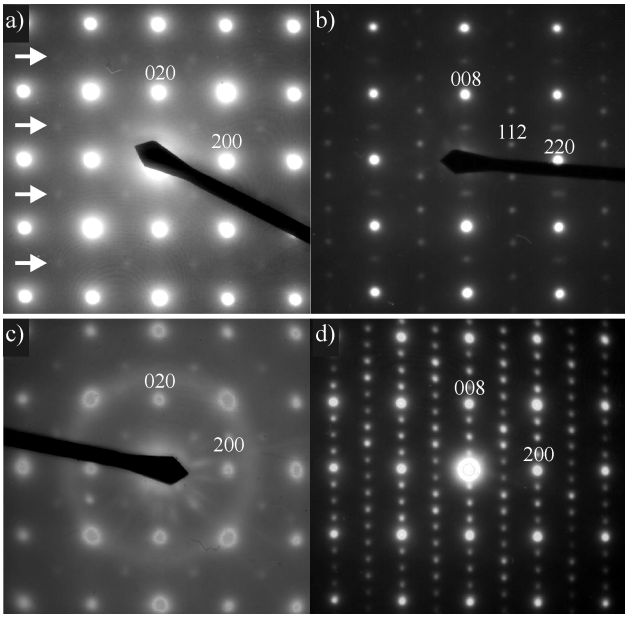

Figure 2. Electron diffraction data collected from (a) the (001) and (b) the ($\bar{1}$10) zone axes of $Ba_4CaFe_3O_{10.7}$; electron diffraction data collected from the (c) (001) and (d) (100) zone axes of $Ba_4CaFe_3O_{9.5}$.

$CaFe_3O_{8-x}$ sheets similar to the $LiSb_3O_8$ sheets present in $Ba_4LiSb_3O_{12}$ shown in Figure 1c.[4] As shown in Figure 3a these cation ordered sheets can be located relative to the cell origin in 4 different ways, corresponding to the Ca^{2+} cations being located at (0,0), (1/2, 1/2), (0, 1/2), or (1/2, 0) within the ab plane of the unit cell to generate 4 distinct layers.

Utilizing space group $I\bar{4}2d$ and locating the calcium and iron cations on 8c crystallographic sites, it is possible to stack the 4 cation ordered layers in two different ways within the unit cell as shown in Figure 3b. In stacking sequence I, each cation ordered layer is stacked adjacent to one identical layer and one dissimilar layer to generate an AACCBBDDAA sequence. In stacking sequence II, each layer is stacked between dissimilar layers to generate an ADCABCDBA sequence. As shown in Figure 3b, these two stacking sequences are simply generated by the symmetry of the space group $I\bar{4}2d$ either by locating the calcium cations at (0,0,$\sim^1/_{16}$) or (1/2, 1/2, $\sim^1/_{16}$) for sequence (I) or (1/2, 0, $\sim^1/_{16}$) or (0, 1/2, $\sim^1/_{16}$) for sequence II. These are the only two stacking sequences which are consistent with unit cell and space groups $I\bar{4}2d$ or $I4_1md$.

To determine which cation ordering scheme is adopted by $Ba_4CaFeO_{10.7}$, structural models were constructed incorporating each of the ordering patterns and then refined against neutron powder diffraction data. During the structural refinements, all atomic positions were allowed to refine as were the fractional occupancies of the anion sites, to account for the oxygen nonstoichiometry of the phase. Comparison of the fits of the two models to the diffraction data showed clearly that model II fits the diffraction data better than model I both statistically (model I, $\chi^2 = 2.63$; model II, $\chi^2 = 1.89$) and visually−the fit using model I contains a large number of diffraction reflections with poor intensity matches between observed and calculated data (see the Supporting Information).

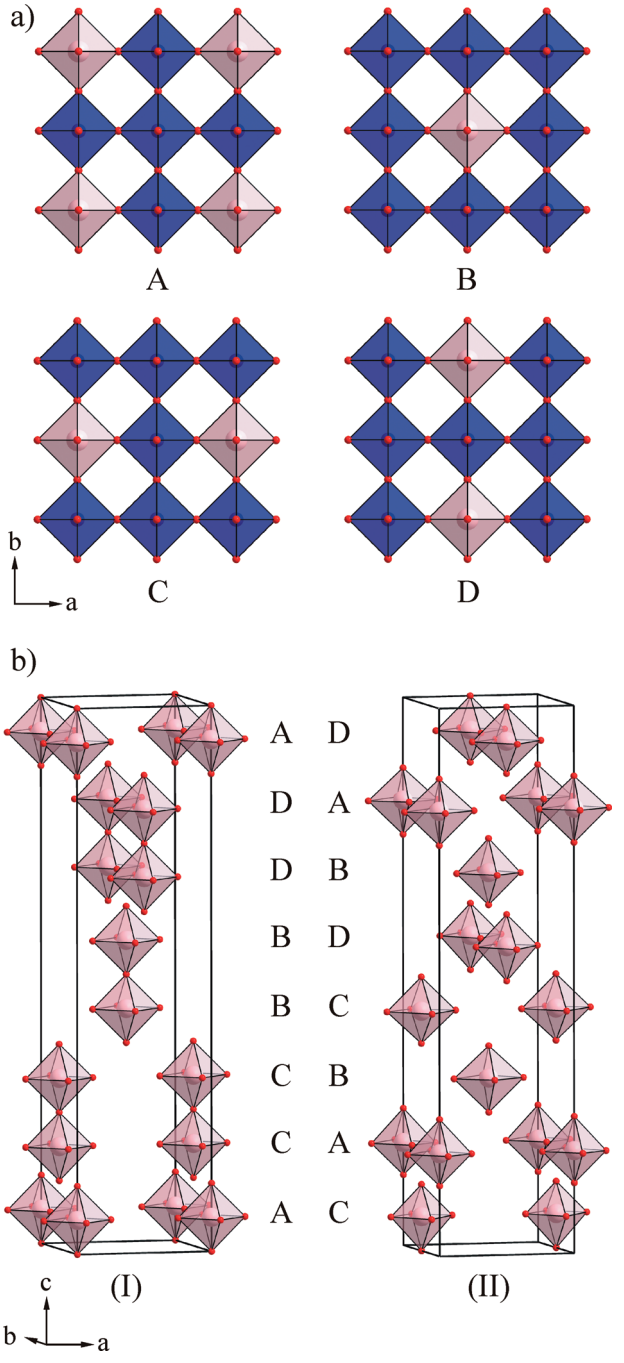

Figure 3. (a) Four possible cation ordered $CaFe_3O_{8-x}$ layers (calcium cations, pink octahedra; iron cations, blue octahedra). (b) Two different stacking sequences of $CaFe_3O_{8-x}$ layers consistent with $I\bar{4}2d$ symmetry. Pink octahedra represent the positions of the calcium cations.

It is clear therefore that model II describes the cation ordering present in $Ba_4CaFe_3O_{10.7}$. Equivalent structural models can be constructed in space group $I4_1md$. Refinement of these models also yield a better agreement between observed and calculated diffraction data for model II rather than model I (model I, $\chi^2 = 2.76$; model II, $\chi^2 = 1.94$); however, the models described in space group $I\bar{4}2d$ have fewer variables and are a better statistical fit to the data and so this description of the structure is retained. A full description of the refined structure of $Ba_4CaFe_3O_{10.7}$ is given in Table 1, with selected bond lengths given in Table 2.

Table 1. Refined Structure of $Ba_4CaFe_3O_{10.7}$[a]

atom	site	x	y	z	fraction	U_{iso} (Å^3)
Ca(1)	8c	1/2	0	0.06239(32)	1	0.024(1)
Fe(1)	8c	0	0	0.06634(7)	1	0.0127(1)
Fe(2)	8c	0	1/2	0.06331(12)	1	0.0127(1)
Fe(3)	8c	1/2	1/2	0.06178(9)	1	0.0127(1)
Ba(1)	16e	0.2507(11)	0.2549(9)	0.00014(1)	1	0.0071(2)
Ba(2)	8d	0.2490(18)	1/4	1/8	1	0.0071(2)
Ba(3)	8d	0.2525(17)	3/4	1/8	1	0.0071(2)
O(1)	4a	0	0	0	0.68(1)	0.0148(2)
O(2)	8c	0	0	0.1286(1)	0.91(1)	0.0148(2)
O(3)	8c	1/2	0	0.9911(1)	1	0.0148(2)
O(4)	4b	1/2	1/2	0	1	0.0148(2)
O(5)	8c	1/2	0	0.1328(1)	1	0.0148(2)
O(6)	16e	0.2199(4)	0.9920(11)	0.0626(1)	1	0.0148(2)
O(7)	16e	0.0049(14)	0.2435(5)	0.0623(1)	0.79(1)	0.0148(2)
O(8)	16e	0.2317(5)	0.5175(8)	0.0633(2)	0.71(1)	0.0148(2)
O(9)	16e	0.4926(12)	0.2793(5)	0.0600(1)	1	0.0148(2)

[a] Space group $I\bar{4}2d$, $a = 8.1821(4)$ Å, $c = 32.3105(19)$ Å; $\chi^2 = 1.89$, wRp = 3.50%, Rp = 5.32%; refinement stoichiometry, $Ba_4CaFe_3O_{10.75(5)}$; titrated stoichiometry, $Ba_4CaFe_3O_{10.71(3)}$.

Table 2. Selected Bond Lengths from the Refined Structure of $Ba_4CaFe_3O_{10.7}$

cation	anion	multiplicity	bond (Å)
Ca(1)	O(5)	2	2.275(11)
	O(6)	2	2.293(3)
	O(9)	2	2.287(4)
Fe(1)	O(1)	1× 0.68	2.143(2)
	O(2)	1× 0.91	2.012(4)
	O(6)	2	1.804(3)
	O(8)	2 × 0.71	1.997(4)
Fe(2)	O(2)	1 × 0.91	1.877(5)
	O(3)	1	1.758(5)
	O(7)	2 × 0.79	2.099(4)
	O(8)	2 × 0.71	1.901(4)
Fe(3)	O(4)	1	1.791(4)
	O(5)	1	1.996(3)
	O(8)	2 × 0.71	2.200(4)
	O(9)	2	1.808(4)

Magnetic Characterization of $Ba_4CaFe_3O_{10.7}$. Neutron powder diffraction data collected from $Ba_4CaFe_3O_{10.7}$ at 5K can be readily fitted by the same structural model as the room temperature diffraction data (see the Supporting Information), indicating there is no long-range magnetic order within the phase down to this temperature. Magnetization data collected as a function of temperature from $Ba_4CaFe_3O_{10.7}$ are shown in Figure 4a. The inset to Figure 4a demonstrates the linear relation between H/M and temperature in the range $50 < T\,(K) < 360$, consistent with Curie−Weiss type behavior. The extracted Curie constant (3.10(5) cm^3 K mol^{-1}) is significantly less than would be expected from a simple paramagnet consisting of a combination of Fe(III) and Fe(IV) centers ($C_{expected} = 12.3$ cm^3 K mol^{-1}). In combination with the sign of the Weiss temperature, this small Curie constant suggests that strong antiferromagnetic interactions exist within the phase but that the disorder in the anion lattice of the material suppresses long-range magnetic order.

Characterization of $Ba_4CaFe_3O_{9.5}$. The systematic absences present in electron diffraction data collected from $Ba_4CaFe_3O_{9.5}$ (Figure 2c,d) correspond to the extinction conditions I _ _ _ . Examination of neutron diffraction

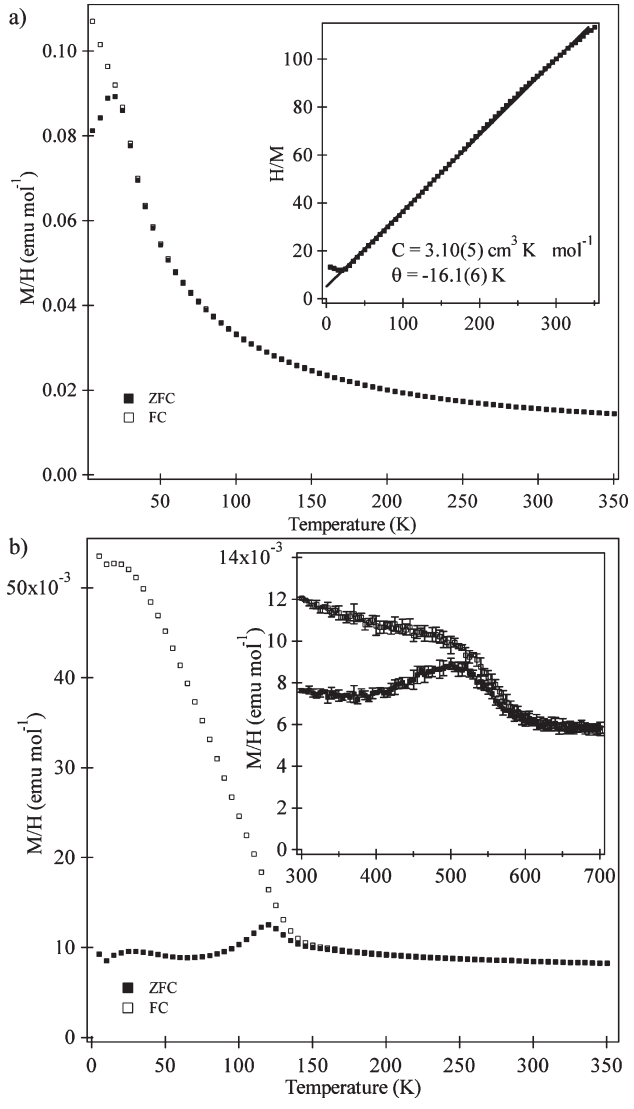

Figure 4. (a) Zero-field-cooled and field-cooled magnetization data collected from $Ba_4CaFe_3O_{10.7}$. Inset shows a linear fit to H/M against T, consistent with the Curie−Weiss law. (b) Zero-field cooled and field-cooled magnetization data collected from $Ba_4CaFe_3O_{9.5}$. Inset shows data collected in the temperature range 300 < T (K) < 700. The anomaly at $T \approx 600$ K is assigned to the onset of (antiferro)magnetic order, with the further anomaly at $T \approx 120$ K assigned to a canting transition of the magnetically ordered phase.

data collected at room temperature from $Ba_4CaFe_3O_{9.5}$ show a series of additional diffraction features at large *d*-spacing that are inconsistent with the body-centered extinction conditions extracted from the electron diffraction data. Magnetization data collected from $Ba_4CaFe_3O_{9.5}$ (Figure 4b) exhibit a magnetic transition at $T \approx 600$ K, suggesting that the additional diffraction features observed in the room-temperature neutron diffraction data are due to magnetic order. Neutron diffraction data collected at 623 K exhibit fewer diffraction peaks than the room-temperature data and are consistent with a body-centered structure, confirming the magnetic origin of the "additional" room-temperature diffraction features. To avoid the complications associated with a simultaneous nuclear and magnetic structural refinement, we performed the structural refinement of $Ba_4CaFe_3O_{9.5}$ against neutron diffraction data collected at 623 K.

A structural model was constructed for $Ba_4CaFe_3O_{9.5}$ in space group $I2_12_12_1$ (an orthorhombic subgroup of the $I\bar{4}2d$ symmetry of $Ba_4CaFe_3O_{10.7}$) based on the refined structure of $Ba_4CaFe_3O_{10.7}$. Because of the way in which the symmetry operations combine in the $I2_12_12_1$ space group, the order of the stacking sequence present in $Ba_4CaFe_3O_{10.7}$ must to be reversed and the origin of the new unit cell shifted in order for the same cation ordered structure to be described. Starting with a model of stoichiometry $Ba_4CaFe_3O_{12}$, the locations of the anion vacancies in $Ba_4CaFe_3O_{9.5}$ were determined by examining Fourier difference plots comparing the structural model and neutron powder diffraction data. The occupancies of anion sites, calculated by the structural model to have too much scattering density, were refined and then further Fourier difference plots calculated. After following this cycle multiple times a model with approximate stoichiometry $Ba_4CaFe_3O_{9.5}$ was refined. This model consisted of a repeating stacking sequence of $-CaFe_3O_7\square-Ba_4O_2\square_2-CaFe_3O_7\square-Ba_4O_3\square-$ (where $\square$ represents an anion vacancy) containing two 6-coordinate calcium sites, two 5-coordinate iron sites, and four 4-coordinate iron sites. At this stage the atomic positions of atoms were allowed to refine. To enhance refinement stability hard constraints were applied forcing the analogous cation coordination sites in the crystallographically distinct $z \approx {}^1/_{16}$ and $z \approx {}^3/_{16}$ $CaFe_3O_7\square$ layers to be identical. As the refinement proceeded these constraints were lifted, allowing the structure to refine freely.

Examination of the displacement parameters of the iron cations revealed those of the Fe(3) and Fe(4) centers were significantly larger than those of the remaining iron centers, suggesting static disorder. To model this, the Fe(3) and Fe(4) centers were moved from the 4c (1/2, 3/4, $\sim{}^1/_{16}$) and (0, 1/4, $\sim{}^3/_{16}$) positions to lower-symmetry 8d (1/2+x, 3/4+y, $\sim{}^1/_{16}$) and (x', 1/4+y', $\sim{}^3/_{16}$) sites with half occupancy. Refinement of these displacements led to an improvement in the statistical fit ($\chi^2 = 1.08$ vs χ^2 1.17). Displacing other iron centers from 4c to 8d sites in an analogous manner did not lead to an improvement in the fit between the model and the data. In addition, when the positions of atoms on these 8d sites were allowed to refine freely, they returned to the high-symmetry 4c positions within error, so the high-symmetry positions were retained. The refinement converged smoothly with good statistical agreement between observed and calculated diffraction data ($\chi^2 = 1.08$). In addition, Fourier difference plots of the final refined model against the diffraction data showed no notable features. A complete description of the refined structure of $Ba_4CaFe_3O_{9.5}$ is given in Table 3 with selected bond lengths in Table 4. Observed, calculated, and difference plots from the structural refinement against data from the three different detector banks are given in the Supporting Information. The complex magnetic ordering of $Ba_4CaFe_3O_{9.5}$ will be described elsewhere.

To confirm the acentric structure refined for $Ba_4CaFe_3O_{9.5}$, we performed powder SHG measurements. The measurements indicated that $Ba_4CaFe_3O_{9.5}$ has a weak SHG efficiency, on the order of α-SiO_2. The weak efficiency may be attributable the dark color of the material,

Table 3. Refined Structure of $Ba_4CaFe_3O_{9.5}$[a]

atom	site	x	y	z	fraction	U_{iso} (Å^3)
Ba(1)	4b	1/4	0.990(5)	0	1	0.0155(4)
Ba(2)	4b	3/4	0.006(5)	0	1	0.0155(4)
Ba(3)	8d	0.236(2)	0.000(3)	0.1267(7)	1	0.0155(4)
Ba(4)	8d	0.767(2)	0.012(2)	0.1193(5)	1	0.0155(4)
Ba(5)	4a	0.766(4)	0	1/4	1	0.0155(4)
Ba(6)	4a	0.268(4)	0	1/4	1	0.0155(4)
Ca(1)	4c	0	1/4	0.0625(3)	1	0.0346(6)
Ca(2)	4c	1/2	3/4	0.1875(3)	1	0.0346(6)
Fe(1)	4c	0	3/4	0.0706(2)	1	0.0281(3)
Fe(2)	4c	0	3/4	0.1793(2)	1	0.0281(3)
Fe(3)	8d	0.572(2)	0.755(2)	0.0669(4)	0.5	0.0305(6)
Fe(4)	8d	0.995(2)	0.277(2)	0.1860(4)	0.5	0.0305(6)
Fe(5)	4c	1/2	1/4	0.0549(2)	1	0.0192(4)
Fe(6)	4c	1/2	1/4	0.1950(2)	1	0.0192(4)
O(1)	8d	0.0212(6)	0.9666(6)	0.0598(3)	1	0.0618(7)
O(2)	8d	0.2833(6)	0.2714(6)	0.0647(4)	1	0.0618(7)
O(3)	8d	0.2163(6)	0.7285(6)	0.1853(4)	1	0.0618(7)
O(4)	8d	0.5214(6)	0.4666(6)	0.1888(3)	1	0.0618(7)
O(5)	4c	0	1/4	0.9956(3)	1	0.0618(7)
O(6)	4c	0	1/4	0.1293(3)	1	0.0618(7)
O(7)	4c	1/2	3/4	0.1206(3)	1	0.0618(7)
O(8)	4c	1/2	3/4	0.2543(3)	1	0.0618(7)
O(9)	8d	0.2501(6)	0.0001(5)	0.0561(4)	0.502(5)	0.0215(6)
O(10)	8d	0.4733(6)	0.9998(5)	0.0750(5)	1	0.0976(5)
O(11)	8d	0.2498(6)	0.2766(6)	0.1720(5)	1	0.0976(5)
O(12)	8d	0.0266(6)	0.0001(6)	0.1948(4)	0.498(5)	0.0215(6)
O(13)	4c	0	3/4	0.1246(8)	1	0.0132(2)

[a] Space group $I2_12_12_1$, a = 8.234(1) Å, b = 8.213(1) Å, c = 34.622(7) Å; χ^2 = 1.08, wRp = 4.01%, Rp = 5.93%; refinement stoichiometry, $Ba_4CaFe_3O_{9.50(1)}$; titrated stoichiometry, $Ba_4CaFe_3O_{9.53(3)}$.

as well as the lack of polarizable cations, e.g., octahedrally coordinated d^0 transition metals and/or lone-pair cations. Although type 1 phase-matching experiments were performed, i.e., SHG efficiency vs particle size, we are unable to state with any certainty the phase-matching capabilities of the material attributable to the weak SHG efficiency.

Discussion

The $Ba_4CaFe_3O_{12-x}$ phases described adopt structures based on that of ABO_3 cubic perovskite, with Ca^{2+} and Fe^{3+} located on the "6-coordinate" B-sites. This is a little unexpected because, for example, the analogous manganese phases $Ba_4Ca_{0.9}Mn_{3.1}O_{11.3}$ and $Ba_7Ca_2Mn_5O_{20}$ adopt hexagonal perovskite structures.[17,18] The structural tolerance factor, t, ($t = \langle A-O\rangle/(\sqrt{2}\langle B-O\rangle)$)[19] gives a good indication of the structure or distortion type a particular ABO_3 perovskite phase will adopt. Using published ionic radii (Ca^{2+} = 1.00 Å, Fe^{3+} = 0.645 Å, Ba^{2+} = 1.61 Å),[20] the calculated tolerance factor for $Ba_4CaFe_3O_{9.5}$ = 0.997, consistent with a cubic perovskite structure.

The anion vacancies present in the structure of $Ba_4CaFe_3O_{9.5}$ adopt an ordered arrangement so that the overall structure can be described as a repeated stacking sequence of $-Ba_4O_2\square_2-CaFe_3O_7\square-Ba_4O_3\square-CaFe_3O_7\square-$ in analogy to the $AO-BO_2-AO-BO_2-$ stacking in the simple cubic perovskite structure. Considering the two B-site cations present, we would expect Ca^{2+}, if it were to be located on a B-site, to strongly favor a coordination number of 6. In contrast, Fe^{3+} is significantly smaller than Ca^{2+} and has a d^5 "spherical" electronic configuration, which means it is likely to adopt sites of lower coordination number with no strong preference for a particular geometry. As shown in Figure 5b, the $CaFe_3O_7\square$ layers within the structure of $Ba_4CaFe_3O_{9.5}$ contain anion vacancies that lead to a 50% occupancy of the *8d* O(9) and O(12) anion sites. As a result, each $CaFe_3O_7\square$ layer contains an array of 6-coordinate octahedral Ca^{2+} centers, 5-coordinate pyramidal Fe^{3+} centers, and 4-coordinate "tetrahedral" Fe^{3+} centers in line with our chemical expectations. Although the location of the anion vacancies in each $CaFe_3O_7\square$ layer leads to disorder in the local coordination sphere of the 4-coordinate iron centers, this disordered arrangement can be considered as the superposition of two equivalent ordered "chains" of FeO_4 centers, which run parallel to the x- or y-axis, as shown in Figure 5b. This suggests that locally each chain of tetrahedra is ordered but that there is no registry between adjacent chains, leading to the three dimensionally disordered structure observed in the diffraction experiment. Bond valence sums (BVS)[21] calculated for the B-site cations within the structure of $Ba_4CaFe_3O_{9.5}$ show evidence for internal strain, as expected for a phase containing B-site cations of such dissimilar size (Table 4). The BVS calculated for the calcium cations are a little larger than expected, consistent with the large Ca^{2+} ions occupying compressed coordination sites. Bond valence sums indicate the iron cations occupy sites under both compression (5-coordinate Fe(5) and Fe(6)) and tension (4-coordinate Fe(1)−Fe(4)). The low values of Fe(3)

Table 4. Selected Bond Lengths from the Refined Structure of $Ba_4CaFe_3O_{9.5}$

cation	anion	multiplicity	bond (Å)	BVS
Ca(1)	O(1)	2	2.336(5)	Ca+2.24
	O(2)	2	2.341(5)	
	O(5)	1	2.316(10)	
	O(6)	1	2.313(10)	
Ca(2)	O(3)	2	2.341(5)	Ca+2.24
	O(4)	2	2.335(5)	
	O(7)	1	2.316(10)	
	O(8)	1	2.313(10)	
Fe(1)	O(1)	2	1.826(5)	Fe+2.77
	O(9)	2 × 1/2	2.130(4)	
	O(13)	1	1.870(42)	
Fe(2)	O(3)	2	1.804(5)	Fe+2.82
	O(12)	2 × 1/2	2.133(4)	
	O(13)	1	1.894(42)	
Fe(3)	O(7)	1	1.873(17)	Fe+2.25
	O(9)	1	1.882(17)	
	O(10)	1	2.079(17)	
	O(10)	1	2.113(17)	
Fe(4)	O(6)	1	1.873(17)	Fe+2.20
	O(11)	1	2.100(18)	
	O(11)	1	2.134(18)	
	O(12)	1	1.885(17)	
Fe(5)	O(2)	2	1.825(6)	Fe+3.34
	O(5)	1	1.748(12)	
	O(10)	2	2.179(11)	
Fe(6)	O(4)	2	1.800(5)	Fe+3.37
	O(8)	1	1.755(12)	
	O(11)	2	2.218(13)	

(17) Schuddinck, W.; Van Tendeloo, G.; Hervieu, M.; Floros, N.; Raveau, B. *Mater. Res. Bull.* **2001**, *36*, 2689.
(18) Floros, N.; Michel, C.; Hervieu, M.; Raveau, B. *J. Solid State Chem.* **2002**, *168*, 11.
(19) Goldschmidt, V. M. *Naturwissenschaften* **1926**, *14*, 477.
(20) Shannon, R. D. *Acta Crystallogr., Sect. A* **1976**, *32*, 751.
(21) Brese, N. E.; O'Keeffee, M. *Acta Crystallogr., Sect. B* **1991**, *47*, 192.

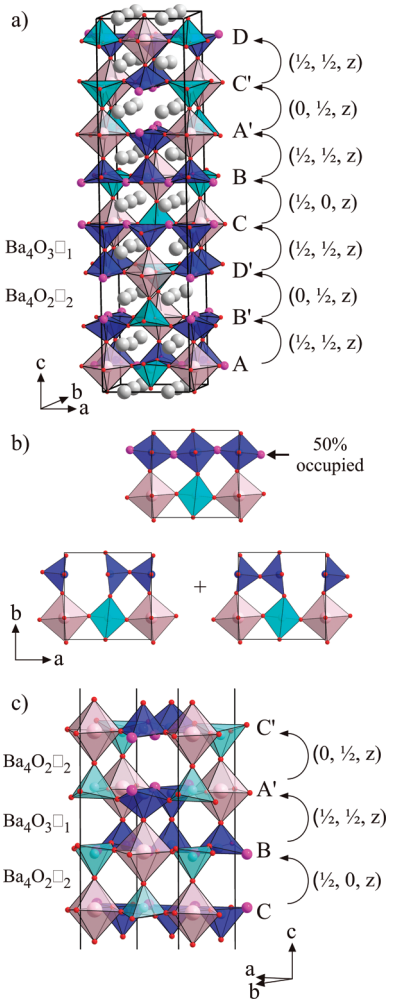

Figure 5. (a) Refined structure of $Ba_4CaFe_3O_{9.5}$. Pink octahedra contain Ca^{2+}; light blue FeO_5 polyhedra contain Fe^{3+}, as do dark blue FeO_4 polyhedra. Gray spheres indicate the position of Ba^{2+} cations. Vectors indicate the relative positions of calcium cations between adjacent layers. (b) Anion vacancy order within $CaFe_3O_7$ sheets. (c) Expanded view of the structure of $Ba_4CaFe_3O_{9.5}$ illustrating the relationship between cation and anion vacancy ordering.

and Fe(4) are also a symptom of disorder, both in the position of these cations and the occupation of their coordination polyhedra, which tends to artificially lower calculated bond valence sums.

Acentric Cation-Order in $Ba_4CaFe_3O_{12-x}$ Phases. The unusual calcium−iron B-site cation order observed in the structures of $Ba_4CaFe_3O_{12-x}$ phases is directed by the interaction between the coordination preferences of the Ca^{2+} and Fe^{3+} cations and the anion vacancy ordering in $Ba_4CaFe_3O_{9.5}$. Examining the way in which the $CaFe_3O_7\square$ layers stack, it can be seen that each CaO_6 site within the structure of $Ba_4CaFe_3O_{9.5}$ shares an 'axial' oxide ion (oxide ions in Ba_4O_{4-x} layers) with one FeO_5 pyramidal site and one FeO_4 tetrahedral site, as shown in Figure 5c. In order to minimize axial bond strain due to bond length mismatches, the anion vacancies within the structure of $Ba_4CaFe_3O_{9.5}$ order such that all oxide ions within each $Ba_4O_2\square_2$ layer bridge between CaO_6 and FeO_5 units as shown in Figure 5c. As a result, each FeO_5 center is connected in a corner sharing manner to three CaO_6 centers − two in an equatorial sense and one in an axial sense across a $BaO_2\square_2$ layer. This connectivity means that pairs of Ca^{2+} cations in neighboring $CaFe_3O_7\square$ layers which are separated by $BaO_2\square_2$ sheets (e.g., the Ca^{2+} cations in layers C and B or A′ and C′ in Figure 5c) have positions related by the vectors (1/2, 0, *z*) or (0, 1/2, *z*). This arrangement also means that the tetrahedral chains in $CaFe_3O_7\square$ layers sandwiching $Ba_4O_2\square_2$ sheets propagate in the same direction as each other, either parallel to the *x*-axis (layers C and B in Figure 5c) or the *y*-axis (layers A′ and C′ in Figure 5c)

Examining the structure of $Ba_4CaFe_3O_{9.5}$ further it can be seen that of the oxide ions in the $Ba_4O_3\square$ layers, 2/3 bridge between CaO_6 octahedra and FeO_5 pyramids with the remaining 1/3 connecting two FeO_4 centers (see the connectivity between B and A′ layers in Figure 5c). As a result of this axial connectivity, the FeO_5 centers (which do not connect across the $Ba_4O_3\square$ sheets) must lie above and below the anion vacancy sites in the $Ba_4O_3\square$ layers. This feature of the structure when combined with the connectivity between CaO_6 and FeO_5 centers described above, forces pairs of Ca^{2+} cations in adjacent $CaFe_3O_7\square$ layers separated by $Ba_4O_3\square$ sheets to have positions related by the vector (1/2, 1/2, *z*). Furthermore, the axial connectivity across the $Ba_4O_3\square$ layers forces the tetrahedral chains in $CaFe_3O_7\square$ sheets either side of these $Ba_4O_3\square$ layers to propagate in orthogonal directions - one parallel to the *x*-axis and one parallel to the *y*-axis as demonstrated by layers B and A′ in Figure 5c.

In combination this means the relative position of the calcium cations within each sequential $CaFe_3O_7\square$ layer stacked along the *z*-axis, is described by the repeating vector sequence: −(1/2, 1/2, *z*)−(0, 1/2, *z*)−(1/2, 1/2, *z*)−(1/2, 0, *z*)−. This cyclic vector sequence naturally generates the 8-layer −A−B′−D′−C−B−A′−C′−D- acentric stacking sequence observed in the structure of $Ba_4CaFe_3O_{9.5}$ (where the difference between layers A and A′ relates to the direction of propagation of the "tetrahedral chains": A parallel to the *x*-axis; A′ parallel to the *y*-axis as shown in Figure 5c). Thus it can be seen that the observed B-site cation ordering of Ca^{2+} and Fe^{3+} in $Ba_4CaFe_3O_{9.5}$ comes from a combination of the coordination preferences of the two cations, the overall oxygen stoichiometry of the phase, and a desire to minimize bond strains to yield a B-cation and anion vacancy ordered structure.

The interactions that lead to the complex chemical order observed in $Ba_4CaFe_3O_{9.5}$ are not unique to this phase and are expected to be present in the majority of anion deficient complex oxides. This suggests that by the judicious selection of pairs of B-cations and careful tuning of the oxygen stoichiometry, a large number of materials with complex cation ordering schemes can be prepared.

The observation of second harmonic generation confirms that the complex cation order present in $Ba_4CaFe_3O_{9.5}$ breaks the inversion symmetry of the cubic perovskite structure. The combination of an acentric crystal structure and paramagnetism/magnetic order (Figure 4b) is highly unusual.[22] Furthermore, if the

(22) Hill, N. A. *J. Phys. Chem. B* **2000**, *104*, 6694.

structure of a material is not just acentric but polar (a subset of acentric structures[23]) it has two of the characteristics necessary to exhibit coupled multiferroic behavior.[24,25] Although in the specific case of $Ba_4CaFe_3O_{9.5}$ the crystal symmetry at room temperature restricts the phase to exhibit piezoelectric behavior rather than pyroelectric or ferroelectric behavior,[23] there is no reason to believe ferroelectric behavior could not be induced into cubic perovskites through complex cation order. Furthermore, because the inversion symmetry in cation ordered phases is broken by the arrangement of cations within the host lattice, rather than by an electronically driven structural distortion (in contrast to $BaTiO_3$ or $BiFeO_3$ for example),[22] we would expect the acentric structures of cation ordered phases to robust with respect to electronic doping. This would allow the magnetic behavior of such phases to be tuned by conventional cation doping, in strong contrast to the vast majority of multiferroic materials currently reported.

(23) Halasyamani, P.; Poeppelmeier, K. R. *Chem. Mater.* **1998**, *10*, 2753.
(24) Eerenstein, W.; Mathur, N. D.; Scott, J. F. *Nature* **2006**, *442*, 759.
(25) Fiebig, M. *J. Phys. D: Appl. Phys.* **2005**, *38*, R123.

In conclusion, through the careful selection of metal cations and the tuning the overall oxygen stoichiometry, complex cation order can be induced into perovskite oxides to yield phases that exhibit both magnetism and acentric crystal structures. Such phases are good candidates to exhibit coupled multiferroic behavior.

Acknowledgment. We thank R. Smith for assistance collecting the neutron power diffraction data at the ISIS facility. Experiments at the ISIS pulsed neutron facility were supported by a beam time allocation from the Science and Technology Facilities Council. J.B. and P.S.H. thank the Robert A. Welch Foundation (Grant E-1457), the ACS PRF 47345-AC10, and the NSF (DMR-0652150) for support.

Supporting Information Available: Observed, calculated, and difference plots comparing the two cation ordering models of $Ba_4CaFe_3O_{10.7}$ against neutron powder diffraction data; observed calculated and difference plots from the refinement of $Ba_4CaFe_3O_{10.7}$ against neutron powder diffraction data collected at 5 K; observed calculated and difference plots from the refinement of $Ba_4CaFe_3O_{9.5}$ against neutron powder diffraction data collected at 623 K (PDF). This material is available free of charge via the Internet at http://pubs.acs.org.